

Dimensional crossover of spin chains in a transverse staggered field: An NMR studyF. Casola,^{1,2,*} T. Shiroka,^{1,2} V. Glazkov,³ A. Feiguin,⁴ G. Dhalle, ⁵ A. Revcolevschi,⁵ A. Zheludev,⁶ H.-R. Ott,¹ and J. Mesot^{1,2}¹Laboratorium für Festkörperphysik, ETH Hönggerberg, CH-8093 Zürich, Switzerland²Paul Scherrer Institut, CH-5232 Villigen PSI, Switzerland³P.L. Kapitza Institute for Physical Problems, RAS, 119334 Moscow, Russia⁴Department of Physics, Northeastern University, Boston, Massachusetts 02115, USA⁵Laboratoire de Physico-Chimie de l'Etat Solide, Université Paris-Sud, 91405 Orsay cedex, France⁶Neutron Scattering and Magnetism, Laboratorium für Festkörperphysik, ETH Hönggerberg, CH-8093 Zürich, Switzerland

(Received 4 July 2012; revised manuscript received 26 September 2012; published 9 October 2012)

Heisenberg spin-1/2 chain materials are known to substantially alter their static and dynamic properties when experiencing an effective transverse staggered field originating from the varying local environment of the individual spins. We present a temperature-, angular- and field-dependent ²⁹Si NMR study of the model compound BaCu₂Si₂O₇. The experimental data are interpreted in terms of the divergent low-temperature transverse susceptibility, predicted by theory for spin chains in coexisting longitudinal and transverse staggered fields. First, our analysis employs a finite-temperature density matrix renormalization group (DMRG) study of the relevant one-dimensional Hamiltonian. Next, we compare our numerical with the presently known analytical results. With an analysis based on crystal symmetries, we show how the anisotropic contribution to the sample magnetization is experimentally accessible even below the ordering temperature, in spite of its competition with the collinear order parameter of the antiferromagnetic phase. The modification of static and dynamic properties of the system due to the presence of a local transverse staggered field (LTSF) acting on the one-dimensional spin array are argued to cause the unusual spin reorientation transitions observed in BaCu₂Si₂O₇. On the basis of a Ginzburg-Landau type analysis, we discuss aspects of competing spin structures in the presence of magnetic order and of the enhanced transverse susceptibility.

DOI: [10.1103/PhysRevB.86.165111](https://doi.org/10.1103/PhysRevB.86.165111)

PACS number(s): 75.10.Pq, 76.60.-k, 75.40.Cx

I. INTRODUCTION

In systems of reduced dimensionality, thermal and quantum fluctuations are the source of physical phenomena without analogues in ordinary 3D materials. Since the original studies of Mermin and Wagner on the role of thermal fluctuations,¹ it is known that in the isotropic spin-*S* Heisenberg model the divergent number of low-energy thermal excitations (i.e., spin waves) suppresses any long-range ordered phase for dimensions $d \leq 2$. Due to the reduced dimensionality, the magnetic properties of spin arrays such as spin chains and ladders are further influenced by quantum effects that are masked in common 3D materials. At $T = 0$, despite quantum corrections present in the antiferromagnetic case, magnetic order develops in the ground state of the 2D bipartite Heisenberg model. Due to the statistical analogy of a quantum d -dimensional antiferromagnet at zero temperature with a purely classical magnet at finite temperature in $d + 1$ dimensions,² quantum effects, particularly effective in the antiferromagnetic case, imply the absence of long-range order in quantum Heisenberg antiferromagnets for $d = 1$.

In real bulk materials, however, the same concept of one-dimensionality is ill defined. For instance, it has often been shown that the effective dimensionality of certain materials can strongly change upon variations of temperature,³ magnetic field,⁴ or energy scale^{5,6} being probed. As a consequence, the interpretation of the experimental observations requires an interpolation between limits of different effective degrees of freedom. This is particularly true for the specific case of spin-1/2 antiferromagnetic (AF) Heisenberg chains realized

in well-known model materials such as KCuF₃,³ Sr₂CuO₃,⁷ or copper pyrazine dinitrate.^{8,9} Their high-temperature disordered phases, well described by the strictly one-dimensional Luttinger Liquid concept,¹⁰ are at low temperatures replaced by a magnetically ordered state induced by weak interchain interactions. The need to interpolate between different dimensionalities suggested the introduction of the class of so-called *quasi*-1D materials. The degree of one dimensionality is usually measured in terms of the ratio between the Néel temperature, marking the onset of the 3D magnetic order, and the intrachain exchange interaction.¹¹⁻¹³ Values of this ratio much below one signify the preservation of the 1D character of the system. Nevertheless, 1D quantum fluctuations continue to be effective in the 3D domain too, i.e., below the Néel temperature. This is evident from both the strongly reduced saturation moment in the ordered state as well as from the deviations with respect to excitations predicted by the standard spin-wave theory.^{14,15} Observations of the evolution of the properties of a physical system across the phase diagram, in regions characterized by different effective dimensionalities, have motivated a number of theoretical and experimental studies, dedicated to the phenomenon of dimensional crossover.

The physics of an assembly of isolated spin-1/2 quantum chains upon increasing the interchain couplings is rather well understood.^{14,16} The impact of such a perturbation on chains experiencing a local transverse staggered field (LTSF), however, is still an open question.¹⁷ A spin-1/2 quantum chain in a uniform field and a concomitant LTSF is usually modeled

by the Hamiltonian:¹⁸

$$\mathcal{H} = J \sum_i \mathbf{S}_i \cdot \mathbf{S}_{i+1} - g\mu_B H \sum_i S_i^z + (-1)^i \mu_B H_{\perp} \sum_i S_i^x, \quad (1)$$

where i is the site index along the chain direction, J is the intrachain exchange coupling constant, μ_B is the Bohr magneton, g is the electronic gyromagnetic ratio, z and x are the directions parallel and perpendicular to the externally applied field H , respectively. The locally induced transverse staggered field is $H_{\perp} = cH$, with c as a constant.

The interest in spin chains with an LTSF was first triggered by experimental studies on copper benzoate $\text{Cu}(\text{C}_6\text{H}_5\text{COO})_2 \cdot 3\text{H}_2\text{O}$,¹⁹ probing the compound's magnetism via susceptibility, nuclear magnetic resonance (NMR) and electron-spin resonance (ESR) measurements. In zero magnetic field ($H = 0$), copper benzoate was known to be just another realization of a spin-1/2 Heisenberg chain, with an exchange constant $J/k_B \sim 18$ K and the onset of a canted antiferromagnetic order at ~ 0.8 K.²⁰ Due to the relatively small intrachain exchange coupling, copper benzoate was considered as a favorable material for studying the field-dependent properties of the 1D spin-1/2 quantum Heisenberg model. However, the field-dependent bulk properties were soon found to be incompatible with corresponding theoretical results.²¹ Incommensurate soft modes at field-dependent reciprocal space positions of the excitation spectrum are expected for spin-1/2 antiferromagnets in an applied field. The first inelastic neutron scattering (INS) experiment, intended to verify these theoretical predictions, was performed on copper benzoate.²² Field-driven incommensurate modes were indeed found at the expected positions in reciprocal space. Due to an unexpected field- and orientation-dependent spin-gap Δ , scaling as $H^{2/3}$, these modes were not soft, however.²² This surprising INS observation was soon interpreted as the result of the particular character of the g tensors and of Dzyaloshinskii-Moriya (DM) interactions. Along the chain direction, the nondiagonal tensor components change sign from one Cu site to the next, and the same is true for the DM \mathbf{D} vector. Both can be mapped onto an effective LTSF and thus to Eq. (1). Formally it turns out that, in the absence of interchain perturbative terms, the effective low-energy theory of the LTSF Hamiltonian is given by the quantum sine-Gordon (SG) model.^{23,24} The SG model is one of the few nonlinear problems that benefits from an exact solution. Hence, the low-energy theory provides analytical expressions for the physical quantities in the temperature range $\Delta < T \ll J$ when $g\mu_B H \ll J$.

In the last 15 years, the magnetic properties of a large number of both organic and inorganic compounds have successfully been described by the LTSF model. Specifically, NMR and ESR studies focused mostly on the joint detection of the temperature-dependent longitudinal [$\propto \langle S_i^z \rangle(T)$] and transverse [$\propto \langle S_i^x \rangle(T)$] local magnetization. Examples are the cases of copper pyrimidine dinitrate^{25,26} and of $\text{BaCu}_2\text{Si}_2\text{O}_7$.²⁷

Quite generally, any real material, unless directly excluded by symmetry arguments, will develop an arbitrarily small LTSF, captured in the H_{\perp} term of Eq. (1), when an external field H is applied. This field-induced LTSF is expected to compete with that developing due to interchain interactions below

the Néel temperature ($T < T_N$). The resulting physics in the limit where both effects are of similar magnitude is currently not clear.¹⁷ One of the few experimental studies where both perturbations on the 1D spin-1/2 Heisenberg model were strong enough to be experimentally visible is an INS experiment on $\text{CuCl}_2 \cdot 2(\text{dimethylsulfoxide})$ (CDC).²⁸ Spin excitations measured at 40 mK showed that the competition leads to the opening of a gap at a nonzero value of the staggered field H_{\perp} , rather than in zero field, as the scaling relation $\Delta \propto H^{2/3}$ would imply. Besides the particular case of CDC, all other ESR and NMR studies of materials modeled by Eq. (1) were usually limited to the range $T > T_N$.

By exploiting the high sensitivity of nuclear magnetic resonance to local magnetic fields, we present a ²⁹Si NMR study of $\text{BaCu}_2\text{Si}_2\text{O}_7$. We demonstrate how the local magnetization in a chain, adequately modeled by Eq. (1), develops above T_N and how it evolves when $T \leq T_N$. The latter evolution could be monitored thanks to the complete decoupling of the local field-induced magnetization from the order parameter which is related to the onset of a standard, temperature-driven second-order magnetic phase transition.

In Sec. II, we briefly summarize relevant results of previous research on $\text{BaCu}_2\text{Si}_2\text{O}_7$. Our NMR data are presented in Sec. III, while a detailed discussion of the analysis is reported in Sec. IV. Finally, Sec. V offers a summary and the main conclusions of this work.

II. $\text{BaCu}_2\text{Si}_2\text{O}_7$: SUMMARY OF PREVIOUS RESEARCH

$\text{BaCu}_2\text{Si}_2\text{O}_7$ crystallizes in the orthorhombic space group $Pnma$ (D_{2h}^{16}) with lattice constants $a = 6.862$ Å, $b = 13.178$ Å, and $c = 6.897$ Å.²⁹ Each unit cell contains eight Cu^{2+} ions, which determine the material's magnetic properties, and eight silicon atoms, each family being equivalent by local symmetry. Both types of atoms, together with the respective closest-oxygen-atom configurations, are depicted in Fig. 1. The copper-ion spins form zigzag chains along the crystallographic c axis. Early zero-field INS studies of $\text{BaCu}_2\text{Si}_2\text{O}_7$ at $T > T_N$ revealed a gapless spinon continuum. A fit to the lower boundary of the spectrum provided an intrachain exchange value $J = 24.1$ meV.³⁰ At the same time, elastic neutron-scattering measurements found evidence of a long-range antiferromagnetic order below $T_N = 9.2$ K, with

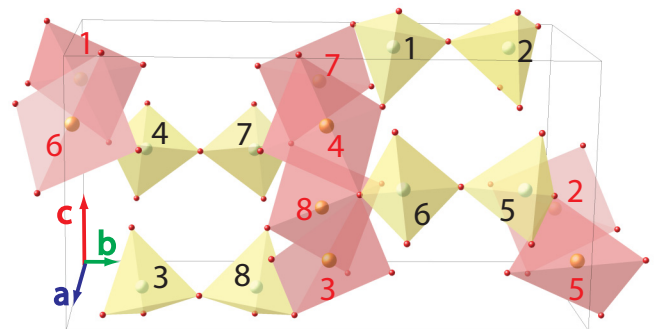


FIG. 1. (Color online) Schematic view of the crystalline unit cell of $\text{BaCu}_2\text{Si}_2\text{O}_7$. Red and black numbers identify the copper and silicon atom sites, respectively. The small red spheres indicate the oxygen sites. Zigzag Cu^{2+} spin chains run along the c axis.

an ordered Cu^{2+} moment at saturation of $0.15\mu_B$, collinear with the c axis.^{13,30} These results qualify $\text{BaCu}_2\text{Si}_2\text{O}_7$ to be among the best realizations of a spin-1/2 Heisenberg chain system, characterized by a low ordering temperature and by a large intrachain exchange coupling. For a global overview of the materials' classification, the reader is referred to Table 1 in Ref. 11. Over the years, studies of $\text{BaCu}_2\text{Si}_2\text{O}_7$ proceeded along two main directions, both related to the present work: (i) the study of the spin-reorientation transitions^{31–34} and (ii) the investigation of the 1D-to-3D crossover.³⁵

Regarding the first topic, experiments employing neutron scattering,^{31,32} ESR,³³ and ultrasound techniques,³⁴ were carried out in externally applied magnetic fields of varying strengths and orientations. These studies provided evidence of a number of phase transitions related to the realignment of spins (and spin-flop transitions for an externally applied field $\mathbf{H} \parallel c$) at $T < T_N$.³⁶ In spite of serious efforts, the cause for these transitions is not yet clear.^{33,36} In the following, we show that NMR data provide direct evidence of the presence of an enhanced transverse susceptibility below T_N , offering a simple explanation for the observed spin reorientations. We suggest that nontrivial phase diagrams below the magnetic ordering temperature may appear naturally in anisotropic quasi-1D antiferromagnets exhibiting a strong reduction of the ordered moment.

As for the second topic, early studies have shown that $\text{BaCu}_2\text{Si}_2\text{O}_7$ is also a model spin-chain compound for investigating the crossover from quantum-spin 1D dynamics to semi-classical 3D (spin-wave) dynamics.^{5,13} Zero-field INS experiments probing the range below the Néel temperature revealed how the presence of weak interchain interactions $J_{\perp} \ll J$, produce an effective LTSF originating from neighboring chains, which leads to a confinement of massless spinon excitations at $T < T_N$. Therefore the situation is not equivalent to that of non interacting 1D chains in a staggered field.

The additional J_2 interactions induce dispersive excitations with a momentum transverse to the chain direction. Their energy vanishes at well defined positions in reciprocal space, coinciding with the Bragg peaks of the ordered structure. For $\text{BaCu}_2\text{Si}_2\text{O}_7$ in an applied magnetic field, intrinsic anisotropies lead to a field-induced LTSF causing a spin gap to be present already above T_N . The possibility of directly measuring the field-induced gap via INS is slim, but important consequences are expected for the local static magnetization. Since the latter is accessible via NMR, we took advantage of this unique opportunity to study the 1D-to-3D crossover in a quantum-spin chain with an LTSF modeled by Eq. (1).

III. NMR EXPERIMENTAL RESULTS

The NMR measurements were carried out on a $4 \times 2 \times 2 \text{ mm}^3$ single crystal of $\text{BaCu}_2\text{Si}_2\text{O}_7$. Since the a and c lattice parameters are roughly the same, the correct identification of the two crystallographic directions is not trivial. Field-dependent magnetization measurements on the same sample with $\mathbf{H} \parallel c$ could detect the two expected spin-flop transitions, hence confirming the correct identification of the crystal axes.

The ^{29}Si NMR lines were measured as a function of temperature at two different magnetic fields, with the external field being applied along the crystallographic a or b axis. Spectra above the antiferromagnetic transition were recorded with a standard spin-echo technique, while at lower temperatures the line intensities were established by a superposition of frequency sweeps as described in Ref. 37. The NMR spectra reported in Fig. 2(a) show the height-normalized shapes versus temperature, measured at 7 T for both crystal orientations. In the paramagnetic phase ($T > T_N$), single lines are observed, which split into two in the ordered regime. While the results are qualitatively the same for both field directions, quantitative differences are obvious. With the field along the

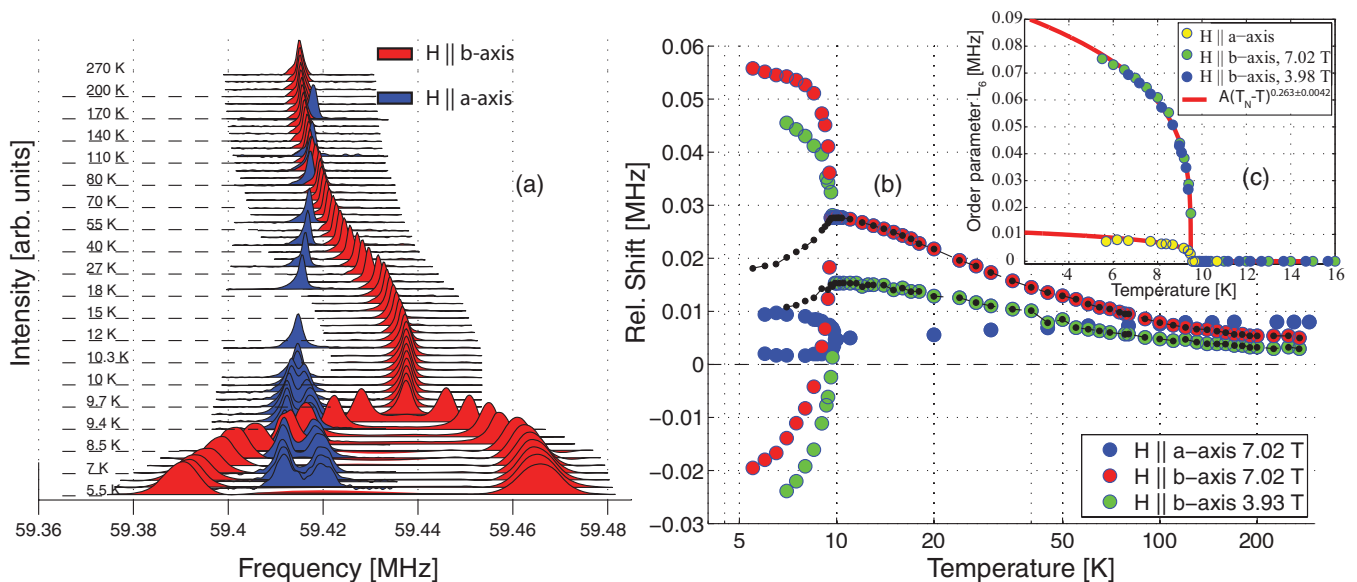


FIG. 2. (Color online) (a) Temperature dependence of NMR ^{29}Si resonances with an applied field \mathbf{H} of 7.02 T along the crystallographic b and a axes. (b) Relative shift of the peak positions as a function of temperature. (c) Direct measure of the order parameter of the antiferromagnetic phase, reflected in the difference of the positions of the split lines. The mean values in the ordered phase are indicated by black dots. The zero frequency marks the resonance frequency of ^{29}Si nuclear spins in a standard reference sample such as $\text{Si}(\text{CH}_3)_4$.³⁸

b axis, the NMR line shifts towards higher frequencies (by approximately 30 kHz) upon lowering the temperature. A much smaller shift is observed when $\mathbf{H} \parallel a$ and, likewise, the line splitting for $T < T_N$ is considerably reduced. The signal width, instead, is approximately the same in both cases and is essentially unaffected across the entire temperature range in the paramagnetic regime.

The monotonic decrease of the resonance frequency with increasing temperature in the paramagnetic phase [see Fig. 2(b)] is quite surprising. A spin-1/2 Heisenberg chain is expected to display a broad maximum in the magnetic susceptibility $\chi(T)$ at $T_{\max} \simeq 0.64J$.³⁹ This maximum, also known as the Bonner-Fisher peak,⁴⁰ should be located at $T_{\max} \simeq 180$ K for $\text{BaCu}_2\text{Si}_2\text{O}_7$ ($J = 24.1$ meV). This was indeed reported in previous works³¹ and confirmed by our low-field magnetization data [see Fig. 5(c)]. Since the NMR line shift and the magnetic susceptibility are generally proportional, the absence of any maximum in Fig. 2(b) for $T > T_N$ is a striking feature, indicating a fundamental difference between the microscopically probed local field (via NMR) and that reflected in the macroscopic susceptibility.

Once the lineshape maxima in the 3D ordered regime ($T < T_N$) were identified [see Fig. 2(b)], the differences between the peak positions, $\Delta\nu$, were evaluated. The corresponding values for the two different orientations are shown in Fig. 2(c). We recall that $\Delta\nu$ is ultimately proportional to the order parameter of the phase transition and hence it can be used to monitor the transition. The resulting increase in frequency splitting between 10 and 5 K can be fitted by a power law $A(T_N - T)^\beta$. Although the chosen temperature range is too broad to really reflect a truly critical regime, the exponent $\beta = 0.263 \pm 0.004$ is very close to $\beta = 0.25$, the value obtained from zero-field neutron diffraction data.¹³ Figure 2(c) clearly confirms that the monotonic increase of the order parameter for $T < T_N$ does not depend on field. Indeed, for $\mathbf{H} \parallel b$, practically the same ordered moment at saturation is found for $\mu_0 H = 3.98$ and 7 T.

The postulated collinear antiferromagnetic order for $T < T_N$ is known to have a zero-field saturation moment of $0.15\mu_B$ and an easy axis which coincides with the *c* direction.^{13,30} As shown in Fig. 2, the line positions reflect the NMR response to a magnetic field oriented along the *a* or *b* direction, respectively, i.e., perpendicular to the easy axis *c*. A standard collinear antiferromagnet with the field applied perpendicular to the easy axis exhibits a constant magnetization in the ordered phase. The NMR lines are thus supposed to split symmetrically with respect to their common relative shift,⁴¹ clearly at variance with our observation. In fact, the average positions of the two maxima, indicated in Fig. 2(b) by full black dots, contrary to expectations, are observed to decrease with decreasing temperature for $T < T_N$. Spin-wave corrections to the constant magnetic susceptibility below T_N for antiferromagnets ordered collinearly along a direction perpendicular to the applied field show at most an increase of the longitudinal magnetization with decreasing temperature. This is due to zero-point spin fluctuations affecting the ordered moment.⁴² However, according to the data presented in Fig. 5(c), this correction is modest in $\text{BaCu}_2\text{Si}_2\text{O}_7$.

The ^{29}Si NMR resonances of $\text{BaCu}_2\text{Si}_2\text{O}_7$ depend strongly on sample orientation, a trend which is particularly

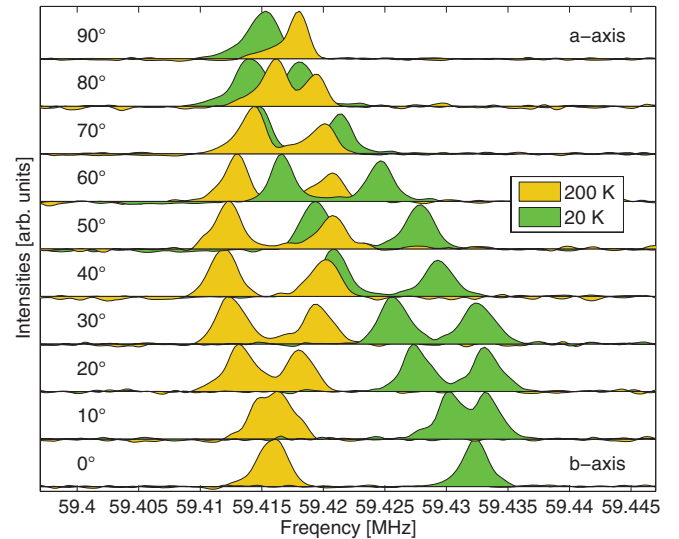


FIG. 3. (Color online) Angular dependence of the NMR lines at 20 and 200 K. The orientation of the external field $\mu_0 H = 7.02$ T varies within the crystalline *ab* plane.

conspicuous in the ordered phase, where the positions and shapes of the NMR lines are sensitive to even a small degree of misalignment. In order to avoid problems with data interpretation due to misorientation, a study to establish the orientation dependence of the NMR lines was carried out by mounting the sample on a two-axis goniometer, suitable for NMR experiments at cryogenic temperatures.⁴³ The results for two temperatures above T_N , 20 and 200 K, are reported in Fig. 3. Once the *a* and *b* axes were identified, the sample was rotated such that the direction of the externally applied field was kept in the *ab* plane of the crystal lattice.

IV. DATA ANALYSIS

After considering the origin of the transverse staggered field (TSF) in Sec. IV A, we discuss the influence of the TSF on the static magnetization by using results of unbiased density-matrix renormalization group (DMRG) calculations in Sec. IV B. The modeling of the NMR lines is described in Sec. IV C, including the calculation of the line shifts in the paramagnetic regime. Experiments and calculations are compared in Sec. IV D. The link to the magnetically-ordered regime is made in Sec. IV E, where we use a Ginzburg-Landau type of analysis to model competing spin structures.

A. Origin of the staggered field in $\text{BaCu}_2\text{Si}_2\text{O}_7$

As already mentioned in Sec. I, the zigzag geometry of the Cu^{2+} spin chains in $\text{BaCu}_2\text{Si}_2\text{O}_7$ provokes electron anisotropies that may strongly affect the physics of the chain system in case of an externally applied magnetic field. Two dominant contributions to the anisotropy originate either in off-diagonal components of the gyromagnetic tensor *g* (alternating in sign along the chain direction) and/or in spin-orbit effects in the Cu-O-Cu superexchange path along the chain. The latter is also known as the Dzyaloshinskii-Moriya (DM) interaction.⁴⁴ To compare the LTSF model of Eq. (1) with experimental data, an estimate of these two contributions to anisotropy has

to be made. A gap in the spin-wave excitation spectrum in the ordered phase was observed in zero-field INS measurements and attributed to two-ion anisotropy effects with an energy scale of ~ 0.4 meV,¹³ while an additional mode at a lower energy of ~ 0.17 meV was observed by ESR.³³ Based on the local symmetry of the intrachain Cu-O-Cu bond, a DM \mathbf{D} vector lying almost in the ab plane, with unit vector components $[0.86, 0.51, 0.07]$ was suggested.³¹

By making use of the crystal symmetry, we apply general space-group operations $\{R_\alpha, \tau_\alpha\}$ to a pair ij of copper sites interacting via oxygen superexchange along the c axis. Rotations R_α and affine transformations τ_α are related to the symmetry operation α . The original pair is transformed into a new set and the local environment transforms accordingly. The configuration of the various \mathbf{D} vectors in the unit cell can be established from the transformation rule:⁴¹

$$\{R_\alpha, \tau_\alpha\} \mathbf{D}_{i,j} = \mathbf{D}_{\{R_\alpha, \tau_\alpha\}i, \{R_\alpha, \tau_\alpha\}j}, \quad (2)$$

where \mathbf{D} transforms as an axial vector under the application of the rotation R_α . With this rule the full pattern of alternating \mathbf{D} vectors, depicted as black arrows, halfway between the relevant Cu sites in the upper panel of Fig. 4, can be derived. We note that the a and b components of the \mathbf{D} vector have alternating signs when moving along a given chain in the c direction, or when moving between different chains in the a direction.⁴⁵

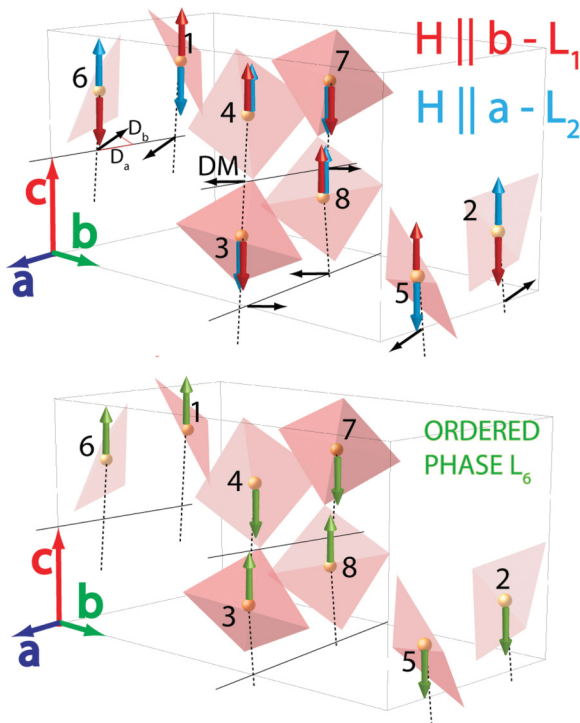


FIG. 4. (Color online) (Top) Pattern of the field-induced LTSF in $\text{BaCu}_2\text{Si}_2\text{O}_7$. Red (blue) lines correspond to the case of a longitudinal field applied along the b (a) axis. The LTSF orientation of sites 3,4,7 and 8 is not affected by the change of field orientation. Black arrows show the direction of the DM vector according to the symmetry rule in Eq. (2) (see text). (Bottom) Local magnetization pattern of the order parameter in the magnetically ordered phase at $T < T_N$ and $\mathbf{H} = 0$. The same kind of structure is realized with a moderate external field in the ab plane.

The effect of the DM interactions between sites i and j , if not forbidden by crystal symmetry, can be taken into account via the following spin Hamiltonian:⁴⁴

$$\mathcal{H}_{\text{DM}} = \mathbf{D}_{i,j} \cdot (\mathbf{S}_i \times \mathbf{S}_j). \quad (3)$$

This contribution can be mapped onto a local transverse staggered field \mathbf{H}_\perp^i via a rotation in spin space.²³ For small $|\mathbf{D}|/J$ ratios, as is the case for $\text{BaCu}_2\text{Si}_2\text{O}_7$, the local transverse field at site i can be approximated by

$$\mathbf{H}_\perp^i \simeq \frac{1}{2J} \mathbf{D}_{j,i} \times g_i^\mu \mathbf{H}, \quad (4)$$

where g_i^μ is the uniform (diagonal) part of the local g tensor valid at site i and \mathbf{H} is the externally applied field. The term in Eq. (4) represents the second type of the LTSF components outlined above.

In addition, strongly orientation-dependent, high-temperature magnetization data were interpreted as indicating a strong anisotropy of the local g tensor.³¹ A direct measurement of the g -tensor components is, in general, possible via ESR experiments. In the case of $\text{BaCu}_2\text{Si}_2\text{O}_7$, however, this is hampered by the broadening and the loss of intensity of the ESR absorption in the paramagnetic phase, providing at best an estimation of $g_b = 2.11 \pm 0.07$ and $g_c = 2.0 \pm 0.1$.³³ The evaluation of the local g tensor is additionally complicated by the strong in-chain exchange interaction, leading to the exchange (or motional) narrowing of the resonance line.⁴⁶ Consequently, differences in the g factor cannot be resolved as long as the corresponding Zeeman splittings are smaller than the exchange energy. Since $J/k_B \simeq 200$ K, this is clearly the case here, even in very strong fields. As a working hypothesis we assume that the g -factor anisotropy is mostly determined by single-ion effects, which reflect the local configuration of oxygen atoms. Figure 1 shows that each copper ion is located at the center of a tetrahedrally distorted CuO_4 square. Because of this distortion, the oxygen-to-oxygen distances of opposite O atoms differ by about 2%. If we neglect this detail, the local point group of the CuO_4 unit is D_{2d} . An arbitrary g tensor is then invariant under all the symmetry operations of the point group D_{2d} . In the local reference frame of a CuO_4 unit, the tensor adopts a uniaxial form $g^{\mu,\nu} = \text{diag}(\tilde{g}_1, \tilde{g}_1, \tilde{g}_9)$, with two of the principal axes oriented along the two directions at 45° from the square's diagonals and the third axis parallel to their cross product. Examples of the transformation matrix and of the resulting parameters $c^i = H_\perp^i/H$ are given in Appendix A.

The configurations of the LTSF, resulting from the orientation of an external field along the crystalline b (a) direction, are indicated by red (blue) arrows in the top of Fig. 4. These patterns are the key for understanding the NMR results. The terms c^i , examples are given in Eq. (A2), are to be inserted in Eq. (1). The two resulting patterns are found to be equivalent to the L_{1c} and L_{2c} irreducible representations of the magnetic-structure space, as previously established in Ref. 47. They consist of the following linear combinations:

$$\begin{aligned} L_{1c} &= S_{1c} - S_{2c} - S_{3c} + S_{4c} + S_{5c} - S_{6c} - S_{7c} + S_{8c}, \\ L_{2c} &= S_{1c} - S_{2c} + S_{3c} - S_{4c} + S_{5c} - S_{6c} + S_{7c} - S_{8c}, \end{aligned} \quad (5)$$

with S_{ic} the component of the local magnetization at the i site along the c axis. Note that the products $L_{1c}H_b$ and $L_{2c}H_a$ are symmetry invariants,⁴⁸ i.e., they are combinations of the irreducible representations (IR) of the magnetic structure that transform according to the trivial representation (the 1D representation consisting of 1×1 matrices containing the entry 1) of the little group of the propagation vector k .⁴⁹

B. Static magnetization of a spin-1/2 chain in a transverse staggered field

As mentioned above the local magnetization at a copper site i , denoted as \mathbf{S}^i , is given by a uniform and a transverse component, such that $\mathbf{S}^i = \mathbf{S}_u^i + \mathbf{S}_\perp^i$, locally induced by an external uniform field $\mathbf{H}_u = g_i^u \mathbf{H}$ and a staggered field \mathbf{H}_\perp^i . In the following, we fix the convention that \mathbf{S}^i has a saturation value of $1/2$. In order to recall the general results already known for \mathbf{S}_u^i and \mathbf{S}_\perp^i and to present our new results, it is useful to introduce the following reduced units:

$$\begin{aligned} h_u^* &= \frac{g_u \mu_B H}{J}, & \chi_u^* &= \frac{\partial \langle S_u \rangle}{\partial h_u^*}, \\ h_{\perp,i}^* &= \frac{\mu_B H_\perp^i}{J}, & \chi_{\perp,i}^* &= \frac{\partial \langle S_\perp^i \rangle}{\partial h_{\perp,i}^*}, & T^* &= \frac{T}{J}. \end{aligned} \quad (6)$$

It has been shown^{50,51} that by using this notation and setting both $h_{\perp,i}^*$ and $h_u^* = 0$, the susceptibility χ_u^* has a peak at $T^* \simeq 0.64$ and a zero-temperature limit of $1/\pi^2$. In Fig. 5(a), we reproduce the temperature dependence of χ_u^* , calculated and tabulated by A. Klümper in Ref. 51. The transverse field h_\perp^* opens a gap in the excitation spectrum which, for $h_\perp^* \ll 1$, scales as⁵²

$$\frac{\Delta}{J} = 1.78(h_\perp^*)^{\frac{2}{3}}(-\ln^{1/6} h_\perp^*). \quad (7)$$

For small fields and $\Delta/J \ll T^* \ll 1$, analytic field-theoretical results for χ_\perp^* are available.²³ In the chosen reduced units, it reads

$$\chi_\perp^* = \frac{0.2779 \ln^{1/2}(T^{*-1})}{T^*}. \quad (8)$$

The high h_\perp^* limit has been treated by previous DMRG calculations.⁵² No complete and unbiased numerical result is yet available for the susceptibility at small magnetic fields across an extended range of T^* . In Figs. 5(a) and 5(b), we fill this gap with results of DMRG calculations^{53–55} for chains with 100 and 200 spin sites, respectively, and compare them with the analytical result of Eq. (8), including or omitting the logarithmic correction. We recall that logarithmic corrections are expected to be effective only at really low temperatures (but still above Δ/J), otherwise they can be safely neglected.²³ In our figure, the subscript α stands for u or \perp , respectively. Without the logarithmic term, the main difference between the analytical and the numerical results is, as expected, at low temperatures. The saturation at low temperatures of the DMRG curves in Fig. 5(b) is due to finite-size effects. In order to see how much a transverse field affects the longitudinal uniform magnetization, we followed Affleck's approach²³ and computed numerically the total derivative $-dF/dh_u^* = m_u$ of the free energy of the system obtaining

$$m_u = \langle S_u \rangle + c^i \langle S_\perp^i \rangle, \quad (9)$$

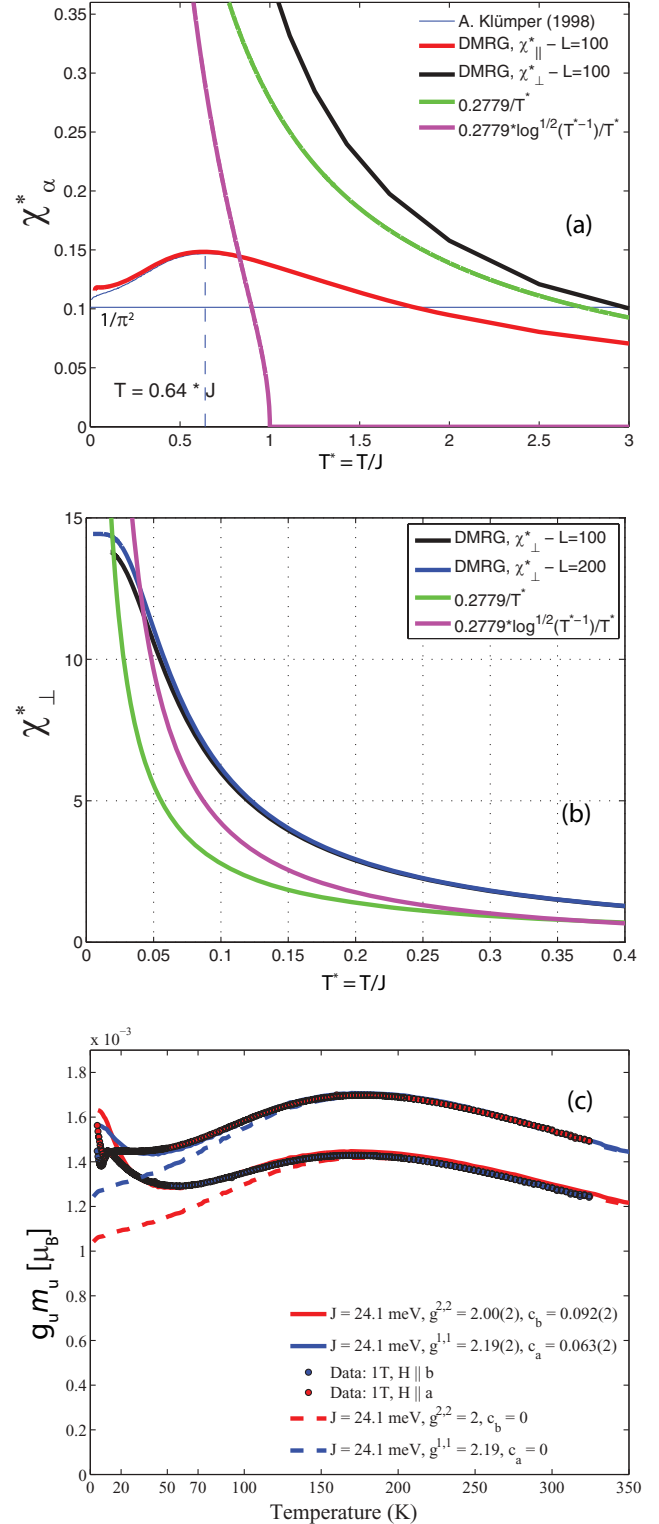


FIG. 5. (Color online) (a) Results of finite temperature DMRG calculations across an extended range of T^* based on Hamiltonian (1) and valid in the small h_\perp^* limit, in comparison with known analytical and tabulated results (see text for details). (b) Comparison of the calculated χ_\perp^* as obtained analytically or via DMRG at $T^* < 0.4$. (c) SQUID-magnetometry data measured at 1 T with the field applied along the a and b crystalline axes, respectively. Solid lines are fits using Eq. (9), dashed lines are predictions for an isotropic uniform chain with no LTSF.

with the parameters c^i as given in Eq. (A2). Two separate DMRG runs were employed to calculate the uniform and staggered susceptibilities independently. Subsequently, Eq. (9) was used to obtain the value of m_u . The possibility to compute the two quantities $\langle S_u \rangle$ and $\langle S_{\perp}^i \rangle$ separately, allowed us to make use of symmetries to reduce the Hilbert space in the DMRG simulations.

In order to compare our simulation results with the data for $\text{BaCu}_2\text{Si}_2\text{O}_7$, the temperature dependence of the magnetization $g_u m_u$ was measured along the a and b axes of the crystal. The data, measured with a SQUID magnetometer, are displayed in Fig. 5(c). Because of the small moment, particular care was taken in the choice of the sample-holder material that would cause at most a small magnetic background signal. With the model given by Eq. (9), we obtain good agreement with the experimental data down to approximately 20 K. The departure of the solid lines from the points is most likely due to approaching the onset of magnetic order. As previous authors,³¹ we also tried a fit by imposing the value $c^i = 0$ (dashed lines). The resulting discrepancies are obvious. From the high-temperature tails of $m_u(T)$, we extract values between 2.19 and 2 for $g^{1,1}$ and $g^{2,2}$, respectively. The latter differ considerably, but are more realistic than the corresponding values between 2.5 and 2.2 quoted in Refs. 30 and 31. Useful information can be extracted from the fit parameters c^i . For the macroscopic uniform magnetization m_u , the sign change of c^i [see Eq. (A2)] is irrelevant. Thus, in Fig. 5(c), c_a and c_b are the corresponding parameters for fields \mathbf{H} along the a or b direction, respectively. First of all, we consider the field-induced and angle-dependent spin gap in Eq. (7). We obtain $\Delta_a = 0.61$ meV and $\Delta_b = 0.78$ meV. These gaps, when expressed in Δ/k_B units, are both of the order of 10 K, i.e., close to the temperature where the magnetic order sets in. This explains why an activated behavior of the spin-lattice relaxation time has not been observed in our previous NMR work.⁵⁶ A proper estimate for the DM parameters $D_{a,b}$ can be obtained by solving Eq. (A2) with $g_1^{\mu,\nu}$ from Eq. (A1) and the fitted $c_{a,b}$. We obtain the values $D_a \simeq 0.94$ meV and $D_b \simeq -1.2$ meV. Remarkably, the ratio $D_a/D_b \simeq 1.25$ is close to 1.68, the value obtained from purely geometrical considerations.³¹ Experimentally it turns out that the NMR response at low temperatures is dominated by the transverse magnetization $\langle S_{\perp}^i \rangle$, i.e., the diverging susceptibility χ_{\perp}^* emerging from the DMRG calculation in Fig. 5(b). The study of this quantity via NMR and its fate below T_N is the main topic of the rest of this paper.

C. Modeling the NMR lines

Having established the contributions to the local magnetic field at the Cu sites, we now proceed to study their influence on the ^{29}Si NMR-line data. In our case, the local magnetization experienced by the silicon nuclei is dominated by the externally applied field, and the contribution due to the sample's magnetization is only of second order. For this reason, the resonance frequency $^{29}\omega_k$ of the ^{29}Si nucleus k ($k = 1, \dots, 8$ —see Fig. 1 for the notation) can be written as⁵⁷

$$^{29}\omega_k \simeq \gamma \frac{\mathbf{H}}{|\mathbf{H}|} \cdot \left[(1 + \sigma_k) \cdot \mathbf{H} + \sum_{i=1}^{\infty} \mathbf{T}_k^i \cdot \mathbf{S}^i + \sum_{i=1}^{NN} \mathbf{A}_k^i \cdot \mathbf{S}^i \right], \quad (10)$$

where γ is the ^{29}Si nuclear gyromagnetic ratio, σ_k is the orbital shift tensor, \mathbf{T}_k^i is the dipolar tensor that couples the silicon nucleus k to the copper atom i , and \mathbf{A}_k^i is the relevant transferred hyperfine interaction. The dipolar sum in Eq. (10) can be calculated directly. This was done by fixing the Cu-spin arrangement resulting from the LTSF configuration shown in Fig. 4 and by including the contributions from the copper atoms within 50 Å from the considered silicon site. The sum of hyperfine interactions runs over the four nearest-neighbor (NN) copper sites.⁵⁶ Given \mathbf{A}_k^i and \mathbf{T}_k^i for the silicon nucleus k , the relevant tensors for the other silicon sites can be obtained by allowed symmetry transformations, meaning that tensors referring to the various silicon nuclei are not mutually independent. If a symmetry operation of the space group $\{R_{\alpha}, \tau_{\alpha}\}$, applied to the silicon site \mathbf{r}_k , brings it to $\{R_{\alpha}, \tau_{\alpha}\}\mathbf{r}_k = \mathbf{r}_{k'}$ (and consequently the copper site \mathbf{r}_i to $\mathbf{r}_{i'}$), the hyperfine tensors are given by $\mathbf{A}_{k'}^i = R_{\alpha}^T \cdot \mathbf{A}_k^i \cdot R_{\alpha}$. Details of the calculation of the hyperfine fields are given in Appendix B.

Next we discuss the two principal results of this section. The first concerns the prediction for the angular-, temperature- and field-dependent relative NMR line shift $\Delta\omega$ in the paramagnetic ($T > T_N$) regime due to the transferred-hyperfine and orbital interactions:

$$^{29}\Delta\omega_{1/2} = \gamma \left\{ \frac{m}{2g_u} [Y_1 g_1^{11} + Y_5 g_1^{22} + (Y_5 g_1^{22} - Y_1 g_1^{11}) \cos 2\theta \right. \\ \left. \pm (Y_2 g_1^{22} + Y_4 g_1^{11}) \sin 2\theta \right] \\ \left. + m^{3/5} (G_3 \sin \theta \pm G_6 \cos \theta) \right. \\ \left. + \frac{1}{2} [\sigma_1 + \sigma_5 + (\sigma_5 - \sigma_1) \cos 2\theta \pm 2\sigma_2 \sin 2\theta] \right\}, \quad (11)$$

where a symmetric orbital-shift tensor σ has been introduced. The consequences of Eq. (11) are discussed in the following section. The model behind Eq. (11) is ultimately independent of the exact geometry of the hyperfine couplings; the qualitative result does not change even if, for instance, the parameters c_{μ} and d_{μ} were zero.

Now we focus on the situation in the *ordered regime*, below T_N . Here, due to the second-order phase transition, the symmetry of the system is spontaneously broken. The adopted order reflects one of the irreducible representations of the magnetic structure. Its product with the applied field is, however, not necessarily an invariant upon symmetry transformations. Consequently, in the ordered regime, the lines are expected to split, even when the field is applied along the main crystallographic axes. From previous zero-field diffraction studies¹³ and following the conventions in Ref. 47, it is known that the representation chosen by the spin system is L_6 , collinear with the c axis (see the lower panel of Fig. 4). By calculating the local field employing Eq. (B5), the NMR lines split below T_N according to

$$h_{1/2,\perp}^{hf} = m_{T < T_N}^{3/5} (\tilde{G}_3 \sin \theta \pm \tilde{G}_6 \cos \theta). \quad (12)$$

Since in the L_6 representation, $m^3 = -m^5$ is always valid, Eq. (12) suggests that the lines should coincide if $\theta = 0$. This is not the case, however, if all the possible silicon sites are considered. In the ordered phase, the local field at the sites $k = 1, 2, 4, 7$ is the same. Also the sites $k = 3, 5, 6, 8$ experience

the same field, but the latter differs slightly from the former. This explains the line splitting shown in Fig. 2 for both field orientations with respect to the crystal axes a and b .

The parameters $\bar{G}_{3/6} = a_{3/6} - b_{3/6} - c_{3/6} + d_{3/6} \neq G_{3/6}$ are not directly accessible by experiment. Nevertheless, Eq. (12) offers the possibility to average out the L_6 contribution to the NMR shift below T_N , thus providing a *direct access* to the components m and m^i of the local magnetization in the ordered regime.

D. Comparison between theory and experiment

As just explained at the end of the previous section, the average NMR line positions at $T < T_N$ [shown as black dots in Fig. 2(b)] are independent of the contribution of the L_6 representation and reflect the influence of the LTSF and the uniform magnetization. This holds true even if a dipolar term

is added to Eq. (11), since the average NMR line position is not affected by the expected symmetrical dipolar splitting below T_N .

With the external field in the ab plane, the LTSF is always collinear with the c axis. For $T > T_N$ the transverse magnetization induced by the LTSF contributes to m_u in the form of Eq. (9). For $T < T_N$, both m and m^i are still present. Since however m [in Fig. 5(c)] is weakly temperature dependent, the strong variation of the average NMR shift for $\mathbf{H} \parallel b$ at $T < T_N$ [see Fig. 6(c)] is dominated by a contribution related to the $L_1(T)$ representation. Thus, below T_N , NMR allows us to reveal the effects of the interaction between the representations L_1 and L_6 . We return to this issue after considering first the $T > T_N$ regime.

The relative shift captured in Eq. (11) includes the anisotropic orbital-shift tensor. Its components along the main crystal axes are usually determined via the so-called

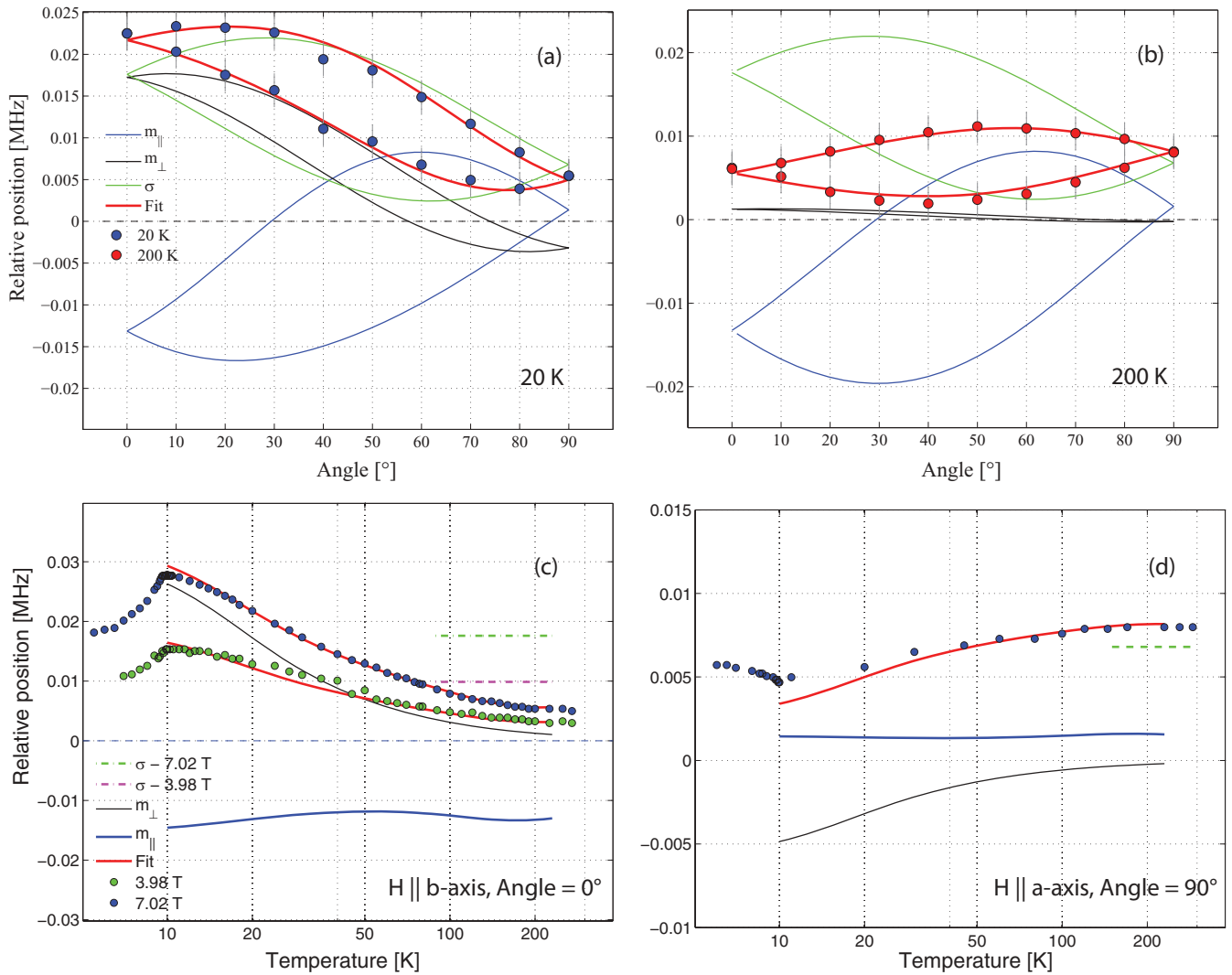


FIG. 6. (Color online) Detailed comparison of the microscopic model captured in Eq. (11) with the experimental ^{29}Si NMR line positions for $T > T_N$. In each panel, the green, black, and blue lines represent individual contributions to the fit related to the orbital shift, the transverse staggered, and the uniform longitudinal magnetizations, respectively. (a) and (b) Angular dependence of the positions of the line maxima with \mathbf{H} in the ab plane, measured at 20 and 200 K (b axis corresponds to $\theta = 0$). (c) and (d) Temperature dependence of the NMR shifts measured with the field applied along the b (left) or a (right) axis. The zero frequency marks the undisturbed resonance frequency of ^{29}Si nuclear spins.

Clogston-Jaccarino plot, where the NMR line shift is plotted versus the corresponding susceptibility.^{25,58} This approach requires a sufficiently broad temperature range, in which the NMR shift mimics the sample's magnetization. Because of the large Cu-O exchange coupling in the BaCu₂Si₂O₇ chains and the weak ²⁹Si NMR signal at elevated temperatures, a reliable estimate of the orbital-shift components was not possible in this way. By assuming this tensor to be symmetric and temperature independent, we released the parameters σ_1 , σ_2 , and σ_5 and the hyperfine couplings. In this way, the whole data set could be fitted with a single set of parameters. The quantitative temperature dependences of m and m^i were established by using the calculations described in Sec. IV B, inserting the values of the LTSF as obtained from the fits in Fig. 5(c).

In Figs. 6(a)–6(d), we display the result of the fits as well as the individual contributions to the local magnetization, as a function of the angle θ and of temperature. In these figures, the individual contributions to the total shift (red curve) of the NMR lines caused by the local longitudinal and transverse magnetizations and by the orbital shift are highlighted as blue, black, and green curves, respectively. For $\mu_0 H = 3.98$ T, only the global fit is presented. Also shown are the temperature independent contributions of the orbital shift [broken lines in Figs. 6(c) and 6(d)]. It may be seen that the temperature dependence of the shift due to the longitudinal magnetization is weak. The transverse component $|m_{\perp}|$ is small at 200 K but it grows significantly at low temperatures. The data were fitted in the range 20 to 230 K. The relative shift of the NMR lines (at very low fields with respect to saturation) scales linearly as a function of field.

The fit parameters we obtain are $Y_1 \simeq 0.014$ T/ μ_B , $Y_5 \simeq -0.16$ T/ μ_B , $G_3 = -0.0752$ T/ μ_B , and $G_6 = 0.1286$ T/ μ_B . Since the fit parameters Y_2 and Y_4 are not linearly independent, we could fit only their combination $Y_2 g^{2,2} + Y_4 g^{1,1} = 0.53$ T/ μ_B . The computed dipolar tensor components, to be inserted in Eq. (11), are of the order of 0.02–0.04 T/ μ_B . The orbital shift values displayed in Fig. 6 are of the order of 150 ppm.

E. Competing spin structures

Employing the same classification of representations as introduced in Ref. 47, the antiferromagnetically ordered phase in zero magnetic field is related to the L_6 representation and the corresponding order parameter. In the previous section, we provided evidence for an enhanced transverse magnetic susceptibility even in the ordered regime. This enhancement is characteristic of quasi-1D chains in an LTSF and we argue that it is the reason for the unusual spin-reorientation transitions that are observed in BaCu₂Si₂O₇. The microscopic approach requires considering the effects of the 1D-to-3D dimensional crossover in specific features of the magnetic properties. In case of chains with no LTSF, this was done with a combined mean-field and random-phase approximation approach.⁵⁹ A mean-field treatment of the case of weakly coupled chains in a transverse field can be found in Ref. 60, but it lacks a detailed comparison with experiment.

Here, we tackle the problem with a Ginzburg-Landau (GL) expansion⁶¹ of the free energy $\bar{\phi}$ close to T_N . Although this phenomenological approach neglects fluctuation effects, it has the advantage of retaining the exchange-energy contributions

to the susceptibility of the ordered phase and includes interactions between different, possibly coexisting, order parameters.

We start by constructing symmetry invariants of the little group of the k vector.⁴⁸ In BaCu₂Si₂O₇, even if exposed to an applied field, a commensurate antiferromagnetic structure with $k = 0$ is realized, leading to a little point group that coincides with D_{2h} . We call $L_{\beta\mu}$ the μ component of $\mathbf{L}_{\beta\mu}$, with \mathbf{L}_{β} the β -IR; clearly the product $\beta\mu = 3N$ (with $N = 8$ as the number of equivalent copper sites in the unit cell). In terms of a GL free-energy expansion over all possible order parameters, a phase transition will occur whenever one of the coefficients A_{β} of the quadratic term $A_{\beta} L_{\beta\mu}^2$ changes sign. Since the L_{6c} representation is the one realized in the magnetically ordered regime in zero field, we can write that $A_6 = \varepsilon_6(T - T_N)$ ($\varepsilon_6 > 0$). All the IRs $L_{\beta\mu}$ of the magnetic structures in BaCu₂Si₂O₇ are one dimensional.⁴⁷ It is therefore easy to construct invariant combinations of the $L_{\beta\mu}$ since the representations of the powers of these terms, which have to transform according to the trivial representation, remain one dimensional. The expansion in Eq. (13) is based on the physics discussed in the previous sections of this paper. Retained are the terms containing $L_{6\mu}$, related to the zero-field magnetic order, $L_{1\mu}$ representing the LTSF, and H the external magnetic field. We will limit our considerations here to the case of an LTSF pattern L_{1c} which is realized for $\mathbf{H} \parallel b$. A more complete analysis will be published separately.⁶² The relevant expansion in powers of $L_{6\mu}$, $L_{1\mu}$, and H_{μ} reads

$$\begin{aligned} \bar{\phi} = & \phi_0 + A_6 \mathbf{L}_6^2 + A_1 \mathbf{L}_1^2 + B_6 \mathbf{L}_6^4 + B_{16} \mathbf{L}_6^2 \mathbf{L}_1^2 \\ & + B'_{16} (\mathbf{L}_6 \cdot \mathbf{L}_1)^2 + D (\mathbf{H} \cdot \mathbf{L}_6)^2 + D' \mathbf{H}^2 \mathbf{L}_6^2 + a_a L_{6a}^2 \\ & + a_b L_{6b}^2 + \alpha_b L_{1c} H_b + \alpha_c L_{1b} H_c - \frac{1}{2} \chi_p \mathbf{H}^2 - \frac{1}{2} \gamma_a H_a^2 \\ & - \frac{1}{2} \gamma_b H_b^2 - \frac{\mathbf{H}^2}{8\pi}, \end{aligned} \quad (13)$$

with ϕ_0 as the value of the free energy in the paramagnetic phase in zero field.

The A_1 coefficient is positive above the Néel temperature, reflecting the absence of a spontaneous symmetry breaking related with the \mathbf{L}_1 representation. On the other hand, we assume A_1 to be small in the vicinity of T_N since, as indicated in Fig. 4, L_{1c} differs from the lowest energy-state configuration L_{6c} only by the mutual orientation of the spins in the neighboring chains, which are relatively weakly coupled. The temperature dependence of A_1 is assumed to be linear in the vicinity of T_N : $A_1 = A_1^{(0)}[1 + \varepsilon_1^{\text{rel}}(T - T_N)]$.

The fourth-order term for L_{6c} fixes the magnitude of the main order parameter below the transition; as required, $B_6 > 0$. The terms with prefactors B_{16} and B'_{16} are crucial in our discussion, because they describe the exchange competition of the field-induced TSF \mathbf{L}_1 and the spontaneous order \mathbf{L}_6 . Microscopically, these terms arise from the simple idea that both the main order parameter and the induced order parameter involve the same local spins, eventually along the same crystallographic direction. The B_{16} coefficient is expected to be positive in order to enhance the energy cost for the coexistence of these two magnetic structures. Finally, the term related to B'_{16} defines the preferred mutual orientation of the two spin patterns by means of the scalar product between them. From the expansion in Eq. (13) alone, it is not possible to predict

whether a collinear ($B'_{16} < 0$) or a transverse ($B'_{16} > 0$) spin configuration is realized.

The terms related to D and D' describe interactions between the longitudinal magnetization and L_6 . The terms with prefactors a_μ describe the orientation of the zero-field order parameter. Reported results of neutron diffraction³² and antiferromagnetic resonance³³ imply that $a_a > a_b > 0$. The term α_b is responsible for the fact that the magnetic structure L_{1c} is induced by an external field applied along the b axis. The powers of \mathbf{H} completing the expansion in Eq. (13) provide a full description of the effects of the g -tensor anisotropy on the longitudinal magnetization. This may be seen by recalling that

$$\frac{\partial \bar{\phi}}{\partial \mathbf{H}} = -\frac{\mathbf{H}}{4\pi} - \mathbf{M}. \quad (14)$$

Minimizing over the components of \mathbf{L}_1 for $\mathbf{H} \parallel b$ and assuming a zero-field collinear antiferromagnetism L_{6c} , we get $L_{1a} = L_{1b} = 0$ and

$$L_{1c} = \frac{-\alpha_b H_b}{2A_1(T) \left[1 + \frac{B_{16} + B'_{16}}{A_1(T)} L_{6c}^2(T) \right]}. \quad (15)$$

With a similar reasoning we obtain the longitudinal magnetization M_b along the b axis, in the former notation denoted as m_u :

$$M_b = -2D(\mathbf{H} \cdot \mathbf{L}_6)L_{6c} - 2D'\mathbf{L}_6^2 H_b - \alpha_b L_{1c} + (\chi_p + \gamma_b)H_b. \quad (16)$$

The last two equations deserve some discussion.

Equation (15) captures the temperature dependence of the transverse staggered magnetization. Microscopically, the increase of L_{1c} upon cooling above T_N ($L_{6c} = 0$) is due to the divergent transverse susceptibility of a 1D spin-1/2 quantum Heisenberg chain in an LTSF. This situation is modeled by the decrease of $A_1(T)$ on cooling (i.e., with $\varepsilon_1^{\text{rel}} > 0$). It also predicts a decrease of L_1 upon the growth of L_6 at $T < T_N$, as observed in the NMR data. Microscopically, the change of regime upon decreasing temperature, from a divergent transverse susceptibility (characteristic of a spin chain) to a progressive competition between the field-induced magnetization pattern and the zero-field order parameter, is argued to be a direct consequence of the dimensional crossover from 1D to 3D of a chain in an LTSF. The clear experimental identification of how 1D physics affects the static magnetization properties even below T_N is the new result emerging from the present study. Below we address the question of how these anomalous properties for $T < T_N$ can explain certain spin reorientation transitions observed in $\text{BaCu}_2\text{Si}_2\text{O}_7$.

By analyzing Eq. (16), we note that the first term is zero for an easy axis (c axis in our case) orthogonal to the direction of the applied field (along the b direction). The second term, instead, provides corrections to the constant magnetization predicted by the standard mean-field theory below T_N . Microscopically, it can be related to a semiclassical contribution of spin-waves.⁴² From the magnetization data in Fig. 5(c), it may be concluded that $D' < 0$. Next, we single out a constant paramagnetic contribution, with prefactors χ_p and γ_b , which is related to the magnetization of the ideal spin-1/2 Heisenberg chain at the Néel temperature. We note that also in this case a contribution from the staggered transverse susceptibility affects the longitudinal magnetization

data, $M(T)$. While L_{1c} scales as $\alpha_b H_b$, the contribution to M_b scales as $\alpha_b^2 H_b$, in full qualitative agreement with the microscopic approach. In magnetization measurements along either the a or the b axis, the contribution of the staggered magnetization matters, but it is not as outstanding as in NMR measurements, where both M_b and L_{c1} are revealed.

The enhanced transverse susceptibility accounts very well for the observed spin reorientations. For example, with the applied field along the b axis, such a transition occurs at $H_{\text{sr}} \simeq 7.8$ T.³⁶ It is caused by a sudden change of the easy axis from the c to the a direction. Below T_N the quasi-one dimensionality extends itself in the form of a field-induced transverse susceptibility. It favors a field-induced spin alignment L_{1c} that competes with the zero-field order parameter L_{6c} . The higher the field, the larger is the energy cost to sustain this arrangement [captured by the term B_{16} of Eq. (13)]. Substituting Eq. (15) into (13) yields an expression that depends on \mathbf{L}_6 only. A spin reorientation is then expected as the result of the competition of the field-dependent anisotropic corrections with the conventional anisotropy of the order parameter at a field:

$$H_{\text{sr}} = \frac{2A_1}{\alpha_b} \sqrt{\frac{a_a}{B'_{16}}}. \quad (17)$$

It can be shown that, for $B'_{16} > 0$, Eq. (13) also accounts for two spin-reorientation transitions when $\mathbf{H} \parallel c$. The inclusion of the staggered field pattern described by the representation L_{2c} [see Eq. (5)] could similarly account for the phase transition at $\mathbf{H} \parallel a$.⁶² Based on formulas (15) and (16), we now attempt a comparison with the experimental data in the temperature range $T < 20$ K, where the microscopic 1D model does not properly describe our results. Using the transferred hyperfine parameters determined in Sec. IVD, we compare the ²⁹Si NMR line shift monitored for a field $H_{\text{sr}} = 7.02$ T oriented along the b axis with the GL approach, postulating $L_{6c} = [(T_N - T)/T_N]^\beta$ and $\beta = 0.5$ (we arbitrarily set the zero-temperature limit of L_{6c} to unity). This is shown in Fig. 7. To obtain tentative estimates of the GL-model parameter, we first fitted M_b of Fig. 5(c) in the vicinity of T_N to Eq. (16) and obtained the parameters $\chi_p + \gamma_b \approx 7.05 \times 10^{-4}$ emu/mol Cu, $D' = -7.6 \times 10^{-5}$ emu/mol Cu and the ratio $\alpha_b^2/(2A_1^{(0)}) \approx 1.05 \times 10^{-4}$ emu/mol Cu. Considering the decrease of L_{1c} with increasing temperature as computed by DMRG above T_N , we obtain $\varepsilon_1^{\text{rel}} = 0.051$ K⁻¹. Next, with the fixed $\alpha_b^2/(2A_1^{(0)})$ ratio we could fit the relative NMR peak positions, as shown in Fig. 7, and hence determine the parameters $A_1^{(0)}$ and $B_{16} + B'_{16}$. The fit shown in Fig. 7 was obtained with $A_1^{(0)} \approx 3.01 \times 10^7$ emu/mol Cu and $B_{16} + B'_{16} \approx 7.3 \times 10^7$ emu/mol Cu. With the present parameters, inserted into the GL model we can obtain, by extrapolation, the value $L'_{1c}(T_N) = 0.15\mu_B\alpha_b H_b/(2A_1^{(0)}) \approx 0.035\mu_B$ for the transverse staggered magnetization at 7.02 T. Notice that in the last relation, we have considered a prefactor 0.15 in the numerator of Eq. (15), corresponding to the experimentally reported zero-temperature limit of L_{6c} expressed in Bohr magnetons, and introduced the identity $L'_{1c}(T_N) = 0.15L_{1c}(T_N)$, whereas L'_{1c} is

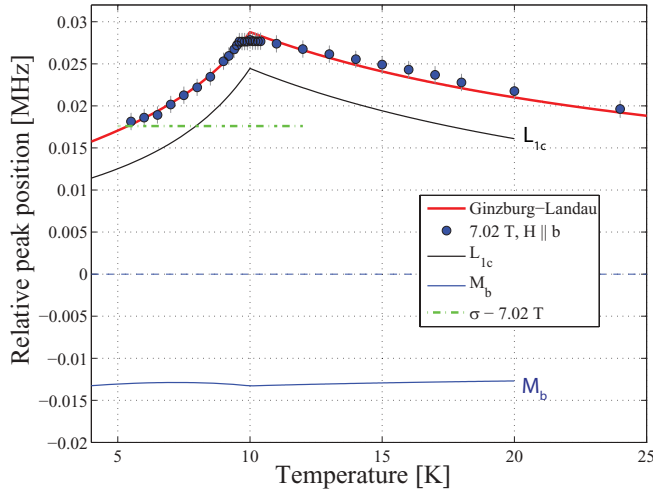


FIG. 7. (Color online) Data representing relative ^{29}Si NMR line shifts in the vicinity of the ordering temperature, compared with the classical predictions of Eqs. (15) and (16). Although fully classical, the GL type approach grasps the competition between the spin structures described by L_{1c} and L_6 . The hyperfine parameters and the orbital shift are taken from the analysis for $T > T_N$ (see text). The average NMR frequency is shown below the transition temperature. Black, blue, and green line show single components of the fits due to L_{1c} , M_b , and σ , respectively.

expressed in absolute and L_{1c} in normalized Bohr magneton units.

Finally, it is instructive to briefly consider the situation encountered in $\text{BaCu}_2\text{Ge}_2\text{O}_7$. Previously obtained magnetization data in low magnetic fields were interpreted as revealing weak ferromagnetism below 8.8 K for $\mathbf{H} \parallel b$.⁶³ It was argued that in the ordered state the interchain coupling along the a axis is of AFM-type and not, as in $\text{BaCu}_2\text{Si}_2\text{O}_7$, of FM-type.²⁹ This implies, however, that the emerging phase below T_N is consistent with the representation L_{1c} and not L_{6c} as in $\text{BaCu}_2\text{Si}_2\text{O}_7$. Consequently, there is no competition between the temperature- and field-induced spin structures, therefore allowing the transverse magnetization L_{1c} to grow in magnitude even below T_N and removing the spin-reorientation transitions for $\mathbf{H} \parallel b$.⁶³ Since for the same field orientation the spin structures above and below the transition temperature coincide, the phase transition in that case is replaced by

$$g_1^{\mu,\nu} = \begin{bmatrix} 0.23\tilde{g}_1 + 0.7\tilde{g}_9 & 0.31(\tilde{g}_1 - \tilde{g}_9) & 0.33(\tilde{g}_1 - \tilde{g}_9) \\ 0.31(\tilde{g}_1 - \tilde{g}_9) & 0.86\tilde{g}_1 + 0.14\tilde{g}_9 & 0.15(\tilde{g}_9 - \tilde{g}_1) \\ 0.33(\tilde{g}_1 - \tilde{g}_9) & 0.15(\tilde{g}_9 - \tilde{g}_1) & 0.84\tilde{g}_1 + 0.15\tilde{g}_9 \end{bmatrix}, \quad (\text{A1})$$

where the subscript i of $g_i^{\mu,\nu}$ refers to the site index. Since the eight copper sites are equivalent under the allowed symmetry operations, we can obtain the tensor $g^{\mu,\nu}$ for each of them. The matrix in Eq. (A1) reveals that the components $g_i^{2,2}$ and $g_i^{3,3}$ are roughly equal (in qualitative agreement with ESR experiments), reflecting the coinciding high-temperature magnetization tails, measured with a field

a simple crossover, characteristic of a ferromagnet in an external field.

V. SUMMARY AND CONCLUSIONS

A detailed analysis of ^{29}Si NMR data obtained by probing single-crystalline $\text{BaCu}_2\text{Si}_2\text{O}_7$ revealed the influence of 1D physics into the regime of 3D magnetic order at temperatures below 10 K. In this way, the problem of weakly interacting nearest-neighbor chains, described in the noninteracting limit by the model in Eq. (1), could be addressed. Based on a classical Ginzburg-Landau analysis, it is shown that in this type of compounds complicated (H, T) magnetic phase diagrams emerge. They are caused by the interaction of the transverse staggered local magnetization, originating from magnetic anisotropies in spin-1/2 Heisenberg chains, with the effective magnetic field due to the weakly ordered spin moments on neighboring chains. We argue that the previously established spin-reorientation transitions in $\text{BaCu}_2\text{Si}_2\text{O}_7$ reflect this situation and can, therefore, be understood in this framework. In the case of $\text{BaCu}_2\text{Ge}_2\text{O}_7$, the lack of competition between field- and temperature-induced spin structures for $\mathbf{H} \parallel b$, also quenches the spin reorientations and changes the phase transition into a crossover phenomenon.

ACKNOWLEDGMENTS

The authors thank K. Prša (EPF Lausanne) and O. Zaharko (PSI) for useful discussions. We are thankful to M. Zhitomirsky (CEA-Grenoble) for the enlightening comments concerning the Ginzburg-Landau approach. This work was financially supported in part by the Schweizerische Nationalfonds zur Förderung der Wissenschaftlichen Forschung (SNF) and the NCCR research pool MaNEP of SNF and in part by the NSF Grant No. DMR-0955707. One of the authors (V.G.) thanks RFBR (Russian Foundation for Basic Research) for the continuous support of his studies and acknowledges hospitality of the Neutron Scattering and Magnetism Group of ETH Zürich that provided precious opportunities to discuss progress of this project.

APPENDIX A: THE g -TENSOR AND THE LTSF PATTERN

Choosing the copper atom 1 in Fig. 1, the transformation matrix relating a CuO_4 unit to the crystallographic unit cell is

along the b and c direction, respectively. The qualitative behavior of the magnetization is also shown in Fig. 1 of Ref. 31.

By considering the g tensor for each site i in the unit cell, and by using Eq. (4) for the DM contribution to the local field, the expected LTSF pattern for an external field applied along the a or b axis can be established. In our case, whenever the

external field lies in the ab plane, the LTSF H_{\perp}^i is found to be parallel to the c direction (see Fig. 4). In order to exploit this favorable configuration, the field orientation $\mathbf{H} \parallel c$ has not been addressed in the present work. With the external field in the ab plane and forming an angle θ with the b axis, we can calculate the ratio H_{\perp}^i/H . For instance, by considering the copper sites 3 and 5, we obtain

$$\begin{aligned} c^3 &= \frac{H_{\perp}^3}{H} = (-g_1^{3,2} \cos \theta + g_1^{3,1} \sin \theta) \\ &\quad + \frac{1}{2J} (-D_a g_1^{2,2} \cos \theta - D_b g_1^{1,1} \sin \theta), \\ c^5 &= \frac{H_{\perp}^5}{H} = (g_1^{3,2} \cos \theta + g_1^{3,1} \sin \theta) \\ &\quad + \frac{1}{2J} (D_a g_1^{2,2} \cos \theta - D_b g_1^{1,1} \sin \theta). \end{aligned} \quad (\text{A2})$$

APPENDIX B: CALCULATION OF THE HYPERFINE FIELDS

An example of a hyperfine tensor is

$$\mathbf{A}_1^3 = \begin{pmatrix} a_1 & a_2 & a_3 \\ a_4 & a_5 & a_6 \\ a_7 & a_8 & a_9 \end{pmatrix} \rightarrow \mathbf{A}_2^5 = \begin{pmatrix} a_1 & -a_2 & a_3 \\ -a_4 & a_5 & -a_6 \\ a_7 & -a_8 & a_9 \end{pmatrix}. \quad (\text{B1})$$

The four NN copper atoms surrounding the silicon atom located at site $k = 1$ are $i = 3, 4, 7, 8$ (see Fig. 1). Contrary to dipolar interactions, the components of the transferred-hyperfine tensor are *a priori* unknown. For calculating directly the θ -dependent component $h_{k,u}^{hf}$ of the uniform local field at site $k = 1$ or 2, parallel to $g^u \mathbf{H}$, we define $\mathbf{A}_1^3 = a_{\mu}$, $\mathbf{A}_1^4 = b_{\mu}$, $\mathbf{A}_1^7 = c_{\mu}$ and $\mathbf{A}_1^8 = d_{\mu}$, and we denote $m = g_u m_u$ and $m^i = g^{3,3} \langle S_i^{\perp} \rangle$. By using the notation of Eq. (B1), we obtain

$$\begin{aligned} h_{k,u}^{hf} &= (\sin \theta \quad \cos \theta) \left[\begin{pmatrix} a_1 & \pm a_2 \\ \pm a_4 & a_5 \end{pmatrix} + \begin{pmatrix} b_1 & \pm b_2 \\ \pm b_4 & b_5 \end{pmatrix} + \begin{pmatrix} c_1 & \pm c_2 \\ \pm c_4 & c_5 \end{pmatrix} + \begin{pmatrix} d_1 & \pm d_2 \\ \pm d_4 & d_5 \end{pmatrix} \right] \frac{m}{g_u} \begin{pmatrix} g_1^{11} & \sin \theta \\ g_1^{22} & \cos \theta \end{pmatrix} \\ &= \frac{m}{2g_u} [Y_1 g_1^{11} + Y_5 g_1^{22} + (Y_5 g_1^{22} - Y_1 g_1^{11}) \cos 2\theta \pm (Y_2 g_1^{22} + Y_4 g_1^{11}) \sin 2\theta], \end{aligned} \quad (\text{B2})$$

where the plus (minus) sign refers to $k = 1$ (2). In Eq. (B2), we take into account that the sample's uniform longitudinal magnetization and the externally applied field may not be collinear due to a possible g tensor anisotropy. By definition, $g_u^2 = (g_1^{1,1} \sin \theta)^2 + (g_1^{2,2} \cos \theta)^2$ and $Y_{\mu} = a_{\mu} + b_{\mu} + c_{\mu} + d_{\mu}$. The reason for picking the Si sites $k = 1, 2$ for describing the relevant NMR line shapes is evident from the contribution of the transverse field $h_{k,\perp}^{hf}$ to the resonance frequency. We get

$$h_{1/2,\perp}^{hf} = (\sin \theta, \cos \theta) \left[m^{3/5} \begin{pmatrix} a_3 \\ \pm a_6 \end{pmatrix} + m^{4/6} \begin{pmatrix} b_3 \\ \pm b_6 \end{pmatrix} + m^{7/1} \begin{pmatrix} c_3 \\ \pm c_6 \end{pmatrix} + m^{8/2} \begin{pmatrix} d_3 \\ \pm d_6 \end{pmatrix} \right]. \quad (\text{B3})$$

In the *paramagnetic phase*, the following relations always hold by symmetry:

$$m^6 = -m^5, \quad m^1 = m^5, \quad m^2 = -m^5, \quad m^4 = -m^3, \quad m^7 = m^3, \quad m^8 = -m^3. \quad (\text{B4})$$

By denoting $G_{3/6} = a_{3/6} - b_{3/6} + c_{3/6} - d_{3/6}$, we obtain for the transverse local field in the paramagnetic phase:

$$h_{1/2,\perp}^{hf} = m^{3/5} (G_3 \sin \theta \pm G_6 \cos \theta). \quad (\text{B5})$$

It turns out that by considering any other of the silicon sites, the only two possible *orthogonal* local fields are those given by Eq. (B5). For an applied field along the a or the b axis, these two local fields coincide. From Eq. (A2), it follows that if $\theta = 0^\circ$ (field along b), $m^3 = -m^5$. The same is true if $\theta = 90^\circ$ (field along a) (see Fig. 4). A single narrow line is thus expected for $\theta = 0^\circ$ and 90° , while two lines are expected in an intermediate angular range and at temperatures exceeding T_N . This is indeed the case, as already shown in Fig. 3.

*fcasola@phys.ethz.ch

¹N. D. Mermin and H. Wagner, *Phys. Rev. Lett.* **17**, 1133 (1966).

²H.-J. Mikeska and A. K. Kolezhuk, in *Quantum Magnetism*, edited by U. Schollwöck, J. Richter, D. J. J. Farnell, and R. F. Bishop, Lecture Notes in Physics (Springer, Berlin, 2004).

³B. Lake, D. A. Tennant, C. D. Frost, and S. E. Nagler, *Nat. Mater.* **4**, 329 (2005).

⁴S. Krämer, R. Stern, M. Horvatić, C. Berthier, T. Kimura, and I. R. Fisher, *Phys. Rev. B* **76**, 100406(R) (2007).

⁵A. Zheludev, M. Kenzelmann, S. Raymond, T. Masuda, K. Uchinokura, and S.-H. Lee, *Phys. Rev. B* **65**, 014402 (2001).

⁶B. Lake, A. M. Tsvetik, S. Notbohm, D. A. Tennant, T. G. Perring, M. Reehuis, C. Sekar, G. Krabbes, and B. Büchner, *Nat. Phys.* **6**, 50 (2009).

⁷K. M. Kojima, Y. Fudamoto, M. Larkin, G. M. Luke, J. Merrin, B. Nachumi, Y. J. Uemura, N. Motoyama, H. Eisaki, S. Uchida, K. Yamada, Y. Endoh, S. Hosoya, B. J. Sternlieb, and G. Shirane, *Phys. Rev. Lett.* **78**, 1787 (1997).

⁸M. B. Stone, D. H. Reich, C. Broholm, K. Lefmann, C. Rischel, C. P. Landee, and M. M. Turnbull, *Phys. Rev. Lett.* **91**, 037205 (2003).

⁹H. Kühne, A. A. Zvyagin, M. Günther, A. P. Reyes, P. L. Kuhns, M. M. Turnbull, C. P. Landee, and H.-H. Klauss, *Phys. Rev. B* **83**, 100407(R) (2011).

- ¹⁰T. Giamarchi, *Quantum Physics in One Dimension* (Oxford University Press, Oxford, 2003).
- ¹¹C. Broholm *et al.*, in *High Magnetic Fields*, edited by C. Berthier *et al.*, Lecture Notes in Physics, Vol. 595 (Springer, Berlin, 2002), pp. 211–234.
- ¹²A. Zheludev, T. Masuda, I. Tsukada, Y. Uchiyama, K. Uchinokura, P. Böni, and S.-H. Lee, *Phys. Rev. B* **62**, 8921 (2000).
- ¹³M. Kenzelmann, A. Zheludev, S. Raymond, E. Ressouche, T. Masuda, P. Böni, K. Kakurai, I. Tsukada, K. Uchinokura, and R. Coldea, *Phys. Rev. B* **64**, 054422 (2001).
- ¹⁴A. Zheludev, *Appl. Phys. A* **74**(Suppl), S1 (2002).
- ¹⁵B. Lake, D. A. Tennant, and S. E. Nagler, *Phys. Rev. Lett.* **85**, 832 (2000).
- ¹⁶F. H. L. Essler, A. M. Tsvelik, and G. Delfino, *Phys. Rev. B* **56**, 11001 (1997).
- ¹⁷B. Xi, S. Hu, J. Zhao, G. Su, B. Normand, and X. Wang, *Phys. Rev. B* **84**, 134407 (2011).
- ¹⁸M. Oshikawa and I. Affleck, *Phys. Rev. Lett.* **79**, 2883 (1997).
- ¹⁹M. Date, H. Yamazaki, M. Motokawa, and S. Tazawa, *Prog. Theor. Phys. Suppl.* **46**, 194 (1970).
- ²⁰D. C. Dender, D. Davidović, D. H. Reich, C. Broholm, K. Lefmann, and G. Aeppli, *Phys. Rev. B* **53**, 2583 (1996).
- ²¹Oshima, K. Okuda, and M. Date, *J. Phys. Soc. Jpn.* **41**, 475 (1976).
- ²²D. C. Dender, P. R. Hammar, D. H. Reich, C. Broholm, and G. Aeppli, *Phys. Rev. Lett.* **79**, 1750 (1997).
- ²³I. Affleck and M. Oshikawa, *Phys. Rev. B* **60**, 1038 (1999).
- ²⁴F. H. L. Eßler, *Phys. Rev. B* **59**, 14376 (1999).
- ²⁵A. U. B. Wolter, P. Wzietek, S. Süllow, F. J. Litterst, A. Honecker, W. Brenig, R. Feyerherm, and H.-H. Klauss, *Phys. Rev. Lett.* **94**, 057204 (2005).
- ²⁶R. Feyerherm, S. Abens, D. Günther, T. Ishida, M. Meiß ner, M. Meschke, T. Nogami, and M. Steiner, *J. Phys.: Condens. Matter* **12**, 8495 (2000).
- ²⁷S. Bertaina, V. A. Pashchenko, A. Stepanov, T. Masuda, and K. Uchinokura, *Phys. Rev. Lett.* **92**, 057203 (2004).
- ²⁸M. Kenzelmann, Y. Chen, C. Broholm, D. H. Reich, and Y. Qiu, *Phys. Rev. Lett.* **93**, 017204 (2004).
- ²⁹Y. Yamada, Z. Hiroi, and M. Takano, *J. Solid State Chem.* **156**, 101 (2001).
- ³⁰I. Tsukada, Y. Sasago, K. Uchinokura, A. Zheludev, S. Maslov, G. Shirane, K. Kakurai, and E. Ressouche, *Phys. Rev. B* **60**, 6601 (1999).
- ³¹I. Tsukada, J. Takeya, T. Masuda, and K. Uchinokura, *Phys. Rev. Lett.* **87**, 127203 (2001).
- ³²A. Zheludev, E. Ressouche, I. Tsukada, T. Masuda, and K. Uchinokura, *Phys. Rev. B* **65**, 174416 (2002).
- ³³V. N. Glazkov, A. I. Smirnov, A. Revcolevschi, and G. Dhalenne, *Phys. Rev. B* **72**, 104401 (2005).
- ³⁴M. Poirier, M. Castonguay, A. Revcolevschi, and G. Dhalenne, *Phys. Rev. B* **66**, 054402 (2002).
- ³⁵A. Zheludev, K. Kakurai, T. Masuda, K. Uchinokura, and K. Nakajima, *Phys. Rev. Lett.* **89**, 197205 (2002); A. Zheludev, M. Kenzelmann, S. Raymond, E. Ressouche, T. Masuda, K. Kakurai, S. Maslov, I. Tsukada, K. Uchinokura, and A. Wildes, *ibid.* **85**, 4799 (2000).
- ³⁶V. N. Glazkov, G. Dhalenne, A. Revcolevschi, and A. Zheludev, *J. Phys.: Condens. Matter* **23**, 086003 (2011).
- ³⁷W. G. Clark, M. E. Hanson, F. Lefloch, and P. Ségransan, *Rev. Sci. Instrum.* **66**, 2453 (1995).
- ³⁸R. K. Harris, E. D. Becker, S. M. Cabral de Menezes, R. Goodfellow, and P. Grangers, *Pure Appl. Chem.* **73**, 1795 (2001).
- ³⁹A. Klümper and D. C. Johnston, *Phys. Rev. Lett.* **84**, 4701 (2000).
- ⁴⁰J. C. Bonner and M. E. Fisher, *Phys. Rev.* **135**, A640 (1964).
- ⁴¹K. Yosida, *Theory of Magnetism* (Springer, Berlin, 1996).
- ⁴²L. J. De Jongh and A. R. Miedema, *Adv. Phys.* **50**, 947 (2001).
- ⁴³T. Shiroka, F. Casola, J. Mesot, W. Bachmann, and H.-R. Ott, *Rev. Sci. Instrum.* **83**, 093901 (2012).
- ⁴⁴I. Dzyaloshinskii, *J. Phys. Chem. Solids* **4**, 241 (1958); T. Moriya, *Phys. Rev.* **120**, 91 (1960).
- ⁴⁵For instance, if we assume $\mathbf{D}_{3,4} = (D_a, D_b, D_c)$ we obtain $\mathbf{D}_{4,3r} = (-D_a, -D_b, D_c) = \mathbf{D}_{8,7}$, $\mathbf{D}_{3,4} = \mathbf{D}_{7,8r}$ and also $\mathbf{D}_{2,1} = (D_a, -D_b, -D_c) = \mathbf{D}_{6,5r}$, $\mathbf{D}_{5,6} = (-D_a, D_b, -D_c) = \mathbf{D}_{1,2r}$. The prime after the index site denotes copper ions belonging to the upper nearest-neighbor unit cell along the c direction.
- ⁴⁶P. W. Anderson, *J. Phys. Soc. Jpn.* **9**, 316 (1954).
- ⁴⁷V. Glazkov and H.-A. Krug von Nidda, *Phys. Rev. B* **69**, 212405 (1974).
- ⁴⁸M. El-Batanouny and F. Wooten, *Symmetry and Condensed Matter Physics*, Chap. 17 (Cambridge University Press, Cambridge, 2008).
- ⁴⁹This is the case when either the space group is symmorphic, or the propagation vector is $k = 0$.
- ⁵⁰D. C. Johnston, R. K. Kremer, M. Troyer, X. Wang, A. Klümper, S. L. Bud'ko, A. F. Panchula, and P. C. Canfield, *Phys. Rev. B* **61**, 9558 (2000).
- ⁵¹A. Klümper, *Eur. Phys. J. B* **5**, 677 (1998).
- ⁵²N. Shibata and K. Ueda, *J. Phys. Soc. Jpn.* **70**, 3690 (2001).
- ⁵³A. E. Feiguin and S. R. White, *Phys. Rev. B* **72**, 220401 (2005).
- ⁵⁴S. R. White, *Phys. Rev. B* **48**, 10345 (1993).
- ⁵⁵S. R. White, *Phys. Rev. Lett.* **69**, 2863 (1992).
- ⁵⁶T. Shiroka, F. Casola, V. Glazkov, A. Zheludev, K. Prša, H.-R. Ott, and J. Mesot, *Phys. Rev. Lett.* **106**, 137202 (2011).
- ⁵⁷A. Abragam, *The Principles of Nuclear Magnetism* (Oxford University Press, Oxford, 1961); C. P. Slichter, *Principles of Magnetic Resonance* (Springer, Berlin, 1990); M.-A. Vachon, G. Koutroulakis, V. F. Mitrović, A. P. Reyes, P. Kuhns, R. Coldea, and Z. Tylczynski, *J. Phys.: Condens. Matter* **20**, 295225 (2008).
- ⁵⁸A. M. Clogston and V. Jaccarino, *Phys. Rev.* **121**, 1357 (1961); A. M. Clogston, V. Jaccarino, and Y. Yafet, *ibid.* **134**, A650 (1964).
- ⁵⁹H. J. Schulz, *Phys. Rev. Lett.* **77**, 2790 (1996).
- ⁶⁰M. Sato and M. Oshikawa, *Phys. Rev. B* **69**, 054406 (2004).
- ⁶¹L. D. Landau and E. M. Lifshitz, *Statistical Physics, I*, Course of Theoretical Physics, 3rd ed., Vol. 5 (Butterworth-Heinemann, Oxford, 1980).
- ⁶²V. Glazkov, F. Casola, H.-R. Ott, and T. Shiroka, [arXiv:cond-mat/1209.4216](https://arxiv.org/abs/cond-mat/1209.4216).
- ⁶³I. Tsukada, J. Takeya, T. Masuda, and K. Uchinokura, *Phys. Rev. B* **62**, 6061(R) (2000).